Electrocatalytic O$_2$-Reduction by Synthetic Cytochrome *c* Oxidase Mimics: Identification of a "Bridging Peroxo" Intermediate Involved in Facile 4e$^-$/4H$^+$ O$_2$-Reduction

Sudipta Chatterjee[†], **Kushal Sengupta**[†], **Shabnam Hematian**[‡], **Kenneth D. Karlin**[‡], and **Abhishek Dey**[†]

Kenneth D. Karlin: karlin@jhu.edu; Abhishek Dey: icad@iacs.res.in

[†]Department of Inorganic Chemistry, Indian Association for the Cultivation of Science, Jadavpur, Kolkata 700032, India

[‡]Department of Chemistry, Johns Hopkins University, Baltimore, Maryland 21218, United States

Abstract
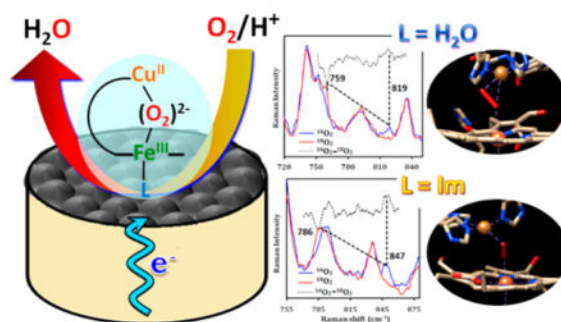
A synthetic heme–Cu C*c*O model complex shows selective and highly efficient electrocatalytic 4e$^-$/4H$^+$ O$_2$-reduction to H$_2$O with a large catalytic rate (>10^5 M^{-1} s^{-1}). While the heme-Cu model (FeCu) shows almost exclusive 4e$^-$/4H$^+$ reduction of O$_2$ to H$_2$O (detected using ring disk electrochemistry and rotating ring disk electrochemistry), when imidazole is bound to the heme (Fe(Im)Cu), this same selective O$_2$-reduction to water occurs only under slow electron fluxes. Surface enhanced resonance Raman spectroscopy coupled to dynamic electrochemistry data suggests the formation of a bridging peroxide intermediate during O$_2$-reduction by both complexes under steady state reaction conditions, indicating that O–O bond heterolysis is likely to be the rate-determining step (RDS) at the mass transfer limited region. The O–O vibrational frequencies at 819 cm^{-1} in ^{16}O$_2$ (759 cm^{-1} in ^{18}O$_2$) for the FeCu complex and at 847 cm^{-1} (786 cm^{-1}) for the Fe(Im)Cu complex, indicate the formation of *side-on* and *end-on* bridging Fe-peroxo-Cu intermediates, respectively, during O$_2$-reduction in an aqueous environment. These

data suggest that *side-on* bridging peroxide intermediates are involved in fast and selective O_2-reduction in these synthetic complexes. The greater amount of H_2O_2 production by the imidazole bound complex under fast electron transfer is due to $1e^-/1H^+$ O_2-reduction by the distal Cu where O_2 binding to the water bound low spin Fe^{II} complex is inhibited.

INTRODUCTION

Cytochrome *c* oxidase (C*c*O), a heme-copper enzyme, catalyzes the $4e^-/4H^+$ reduction of O_2 to H_2O in the terminal step of the electron transport chain during respiration.[1–4] The investigations of oxygen reduction by synthetic heme-Cu models are also related to fuel cell cathode catalysts as they provide fundamental insight into the factors that lead to efficient O_2 reduction materials. C*c*O has attracted paramount interest of synthetic inorganic and bioinorganic chemists due to its great fundamental and practical importance in understanding dioxygen activation/reduction, and proton translocation, etc.[5–10] The X-ray structures of C*c*O reveal the active site responsible for O_2 binding and reduction, to be a binuclear site comprising of heme-a_3, with a proximal histidine (His) along with a distal side histidine bound copper (Cu_B).[3,11,12] One of these three ligating His residues is covalently cross-linked to a nearby tyrosine (Tyr) residue which is said to act as a source of electron and proton in the reduction of O_2 and proton translocation.[13,14] This chemistry stems from the characterization of an intermediate P_M (ferryl $Fe^{IV}=O$ and $Cu^{II}-OH/H_2O$), formed after the O–O bond cleavage in C*c*O, which suggests the presence of a Tyr radical.[15,16] Recent literature suggests that O_2 initially binds to Cu_B (at an overall rate $\sim 10^8 \text{ s}^{-1}$) which is then readily transferred to heme-a_3 (at an overall rate $\sim 10^5 \text{ s}^{-1}$) forming an initial Fe–O_2 adduct analogous to oxy-hemoglobin/myoglobin.[2,14,17] A bridging peroxide $Fe^{III}-(O_2)^{2-}-Cu^{II}$ (either *side-on* or *end-on*) intermediate preceding P_M has been characterized spectroscopically and structurally in some C*c*O active sites; their relevance in catalytic O_2 reduction, while invoked in a few investigations, is not clear (Figure 1).[18–24]

The investigation of synthetic heme-Cu systems has greatly assisted our understanding of the reaction mechanism of dioxygen reduction and factors that lead to selective $4e^-/4H^+$ reduction of O_2 avoiding formation of detrimental partially reduced oxygen species (PROS).[19,26–30] While Collman and coworkers have reported the initial formation of an Fe–O_2 adduct followed by P_M-like intermediate formation with their functional C*c*O model under rate limiting conditions,[27,26] Karlin's group have stressed on the formation of a bridging peroxide as a possible intermediate during O_2-reduction under single turnover conditions.[19,31–33] These bridging peroxo intermediates can also be interconverted, in some cases, from a *side-on* to an *end-on* product in synthetic myoglobin[34,35] or C*c*O models[18,29,32] upon incorporation of an external strong field ligand like imidazole or its analogues. In spite of obtaining significant knowledge and insight into the O_2 reduction mechanism under single turnover conditions in organic solvents, the mechanistic details in an aqueous environment remains unresolved due to the lack of direct spectroscopic evidence, which motivates our present study.

Examples of electrocatalytic O_2-reduction reactions (ORR) employing synthetic C*c*O model complexes containing Fe-only and Fe–Cu centers have been reported at physiological

pH.[29,30,36] Although the presence of Cu ion was initially thought to be essential for selective $4e^-$ reduction of O_2, it has now been established that the presence of Cu is only necessary when the electron transfer (ET) from the electrode is slow.[26,28] The presence of a strong sixth ligand coordinated to the heme center may influence and alter the ORR reactivity. Recently, an experimental setup has been developed where dynamic electrochemistry (rotating disk electrochemistry; RDE) is coupled to a powerful spectroscopic tool, surface enhanced resonance Raman spectroscopy (SERRS) which allows direct *in situ* investigations of the reactive intermediates formed under steady state conditions and thus aids the elucidation of the reaction mechanism for electrocatalytic ORR.[37]

In this study, the electrocatalytic O_2-reductions of a heme-copper [6]L-FeCu complex (**2**, Figure 2) and its imidazole adduct [6]L-Fe(Im)Cu (**3**, Figure 2) have been investigated at physiological pH under steady state conditions, in order to (i) evaluate the efficiencies of this group of complexes under aqueous conditions and (ii) detect intermediates formed during O_2-reduction. Results from study of the Fe-only complex (**1**, Figure 2) serve as a control to evaluate the role of the copper. We find that **1** and **2** selectively reduce O_2 to H_2O under fast electron-transfer (ET) flux, while **3** is less selective in doing so under similar conditions. In fact, the production of PROS decreases with a decrease in ET rate for complex **3** in contrast to complexes **1**, **2** and all other reported Fe–Cu systems.[6,26,28,38–40] The SERRS and SERRS-RDE techniques employed here not only allow identification of intermediates and probable ORR mechanism, but also help to deduce ratedetermining steps, supplementing the information obtained from electrochemical data alone.

RESULTS AND ANALYSIS

Cyclic voltammetry (CV) of complex **1**, which has been physiabsorbed on an edge plane graphite (EPG) electrode in deoxygenated pH 7 phosphate buffer, shows a reversible $Fe^{III/II}$ couple at -210 mV (Figure 3A, blue). Complex **2** shows two reversible CV waves at -155 and 173 mV, which may be ascribed to the $E_{1/2}$ for the $Fe^{III/II}$ and $Cu^{II/I}$ processes, respectively (Figure 3A, red). The $E_{1/2}$ for the $Fe^{III/II}$ couple of **1**, which has an OH^- as the axial ligand, appears at a more negative potential than **2**. Moreover, the presence of distal Cu site in complex **2** is responsible for slight positive shift in $Fe^{III/II}$ potential compared to complex **1**. The CV of **2** obtained here on EPG under aqueous condition is different from that in other C*c*O models obtained in aqueous or organic media, where both the $Fe^{III/II}$ and $Cu^{II/I}$ CV waves appear at same potentials.[19,28] The CV of **3** indicates that the $E_{1/2}$ for the $Fe^{III/II}$ and $Cu^{II/I}$ processes, though very close, are somewhat distinguishable in the cathodic process but overlap completely in the anodic reaction (Figure 3A, green). Therefore, it is quite ambiguous to extract the respective $E_{1/2}$ values from the CV data. The $E_{1/2}$ values for the two processes appear at more negative potentials compared to complex **2**.[41] This is likely due to the binding of imidazole as the sixth ligand to the Fe center (when one equivalent of imidazole is added externally to complex **2**, it binds to the Fe site only as observed from the distinct resonance Raman signal in homogeneous medium; see Figure S1, Supporting Information and the Experimental Details section) which weakens trans Fe–O bond, strengthening the Cu–O bond in this complex, which lowers the $E_{1/2}$ values of both the Fe and Cu centers compared to those in complex **2**. Note that in C*c*O as well as in its synthetic mimics (where imidazole is covalently bound to heme center), the heme and Cu

ion potentials are almost the same.[28,26] Integration of the charge yields the surface coverage, i.e., the number of the electroactive species present on the electrodes. Complexes **1** and **2** show coverages of $(2.36 \pm 0.33) \times 10^{-11}$ and $(1.3 \pm 0.05) \times 10^{-11}$ mol/cm^2 integrating the Fe$^{III/II}$ redox process, respectively. Analogously, the coverage of Cu in the ^{6}L-FeCu is estimated to be $(0.97 \pm 0.06) \times 10^{-11}$ mol/cm^2 implying that the Fe:Cu ratio in complex **2** is close to 1:1, consistent with the formulations of the complex. Note that the individual coverage of Fe and Cu in complex **3** cannot be determined due to overlapping of the Fe$^{III/II}$ and Cu$^{II/I}$ redox processes (Figure 3A, green). However, the total integrated charge of $(2.08 \pm 0.12) \times 10^{-11}$ mol/cm^2 for complex **3** is two times greater than the individual coverage of Fe and Cu obtained for complex **2** consistent with the presence of two electroactive redox centers in **3**.

SERRS was performed on the catalysts **1**, **2** and **3** immobilized on C$_8$SH self-assembled monolayer (SAM) modified roughened Ag surfaces. SERRS data were obtained, both when the catalysts were in their respective resting oxidized state and also under reducing conditions in aqueous pH 7 buffer. SERRS data for **1** under resting conditions exhibits oxidation state (ν_4), coordination number (ν_3) and spin state (ν_2) marker bands at 1362, 1439, and 1556 cm^{-1}, respectively, indicating the presence of a five-coordinated (5C) Fe^{III} high-spin (HS) species on the surface (Figure 3B, red).[42,43] Upon reduction, the formation of a HS Fe^{II} species, having the ν_4 and ν_2 bands at 1347 and 1543 cm^{-1}, respectively, is observed (Figure 3B, green and Figure S2, Supporting Information).[40,42,44,45] The SERRS spectrum of **2** at oxidizing potentials (0 V vs Ag/AgCl), i.e., under resting conditions has the ν_4, ν_3, and ν_2 bands at 1365, 1451, and 1566 cm^{-1}, respectively, which correspond to a six-coordinated (6C) low-spin (LS) Fe^{III} species (Chart 1 and Figure 3C, red). Upon reduction, new ν_4, ν_3, and ν_2 bands at 1347, 1436, and 1544 cm^{-1} are observed which correspond to a HS Fe^{II} species (Chart 1, Figure 3C, green, and Figure 3E).[46] SERRS data of **3** at oxidizing potential show the ν_4, ν_3, and ν_2 bands at 1367, 1453, and 1568 cm^{-1}, respectively, indicating the presence of a 6C Fe^{III} LS species (Chart 1 and Figure 3D, red). This complex **3**, when reduced, mainly leads to the formation of a LS Fe^{II} species with the ν_4, ν_3, and ν_2 bands at 1358, 1447, and 1559 cm^{-1}, respectively (Chart 1 and Figure 3D, green). However, a Lorentzian fit of this reduced spectrum shows the presence of some HS Fe^{II} component as well (Figure 3F).

In the case of complex **2**, the resting oxidized state is observed to be LS when immobilized on the electrode (Figure 3C) unlike in an organic solvent where it is high spin.[33] The change in spin state in **2** is likely due to the fact that complex **2** binds water (from bulk solvent) as an axial ligand (Chart 1). However, for complex **3** the sixth position has already been occupied by the external imidazole ligand before immobilization and it is LS in both organic solvent and aqueous medium (Chart 1, Figure 3D and Figure S1A, Supporting Information). Upon reduction, Fe^{II} HS and Fe^{II} LS species have been obtained as the major components for complexes **2** and **3**, respectively. Hence, it may be proposed that these two complexes exist as 5C water bound Fe^{II} HS and Im-water bound 6C Fe^{II} LS, respectively (Chart 1, right panel) when reduced. A similar distribution of components along with their assignments has been observed previously in SERRS experiments with similar Fe-porphyrin complexes.[38,40]

Note that imidazole and water bound LS Fe^{II} species, although proposed in some synthetic systems, are yet to be structurally characterized.[47,48]

The electrocatalytic O_2 reduction using complexes **1**, **2** and **3** has been investigated using the rotating disk electrochemistry (RDE) technique in air-saturated pH 7 buffer. Linear sweep voltammetry (LSV) of the complexes at different rotation rates shows a substrate diffusion limited catalytic O_2-reduction current below −100 mV vs Ag/AgCl (Figure 4). This current increases with increasing rotation rates following the Koutecky–Levich (K–L) equation, $I^{-1} = i_K(E)^{-1} + i_L^{-1}$, where $i_K(E)$ is the potential dependent kinetic current and i_L is the Levich current where i_L is expressed by $0.62nFA[O_2](DO_2)^{2/3}\omega^{1/2}v^{-1/6}$ and n is the number of electrons transferred to the substrate, A is the macroscopic area of the disk (0.096 cm^2), $[O_2]$ is the concentration of O_2 in an air saturated buffer (0.26 mM) at 25 °C, DO_2 is the diffusion coefficient of O_2 (1.8×10^{-5} cm^2 s^{-1}) at 25 °C, ω is the angular velocity of the disk and v is the kinematic viscosity of the solution (0.009 cm^2 s^{-1}) at 25 °C.[49,50] From the slope of a plot of I^{-1} versus the inverse square root of the angular rotation rate ($\omega^{-1/2}$), the number of electrons delivered to the substrate during electrocatalytic ORR can be evaluated. The slopes obtained from the experimental data for catalysts **1** and **2** are almost identical to the theoretical slope predicted for a 4e$^-$ O_2 reduction process (Figure 4B, D). However, for complex **3**, the slope corresponds to a 3.4e$^-$ process (Figure 4F). The values of n obtained indicate that under conditions of very fast electron transfer (as occurs on EPG electrodes), O_2 undergoes almost complete 4e$^-$ reduction to H_2O when catalyzed by **1** and **2** but not by **3** (vide infra). The second order rate of catalysis (k_{cat}) for ORR can also be obtained from the intercept of this K–L plot using the formula: $i_K = nFAk_{cat}\Gamma_{cat}[O_2]$. The k_{cat} values are obtained to be $(3.65 \pm 1.1) \times 10^6$, $(4.49 \pm 0.9) \times 10^6$, and $(1.28 \pm 0.11) \times 10^6$ M^{-1} s^{-1} for complexes **1**, **2**, and **3**, respectively. These facts indicate that the selectivity and efficiency for 4e$^-$/4H$^+$ O_2-reduction are better for the FeCu complex as compared to its imidazole adduct. It should be noted that the second order rate constant of 4e$^-$/4H$^+$ ORR by complex **2** is 1 order of magnitude greater than FeCu complexes reported earlier.[6,28] The slower reactivity of those synthetic heme-Cu systems may be due to a slower rate of O_2 binding to the 6C LS reduced iron center.[28,47,51]

The selectivity of this electrocatalytic O_2 reduction by the catalysts **1**, **2** and **3** and its dependence on the ET rate from the electrodes has been further evaluated by rotating ring disk electrochemistry (RRDE).[26,28,38,52] Physiabsorption of the catalysts on EPG, C_8SH modified Au and $C_{16}SH$ modified Au electrodes allows fast ($k_{ET} > 10^5$ s^{-1}), moderate ($k_{ET} \sim 10^3$ s^{-1}) and slow ($k_{ET} \sim$ 4–6 s^{-1}) electron transfer fluxes, respectively.[26,53] RRDE measures the amount of PROS produced (*in situ*), if any, due to incomplete O_2 reduction. The amount of PROS produced at pH 7 by **1** under fast, moderate, and slow electron fluxes are $6 \pm 1\%$, $9 \pm 0.5\%$, and $23 \pm 3\%$, respectively (Figure 5 and Figure S3, Supporting Information). We find that with the "extra" redox center, the copper ion in complex **2**, PROS quantities decrease, compared to **1**, and the difference in PROS production is more prominent under slow electron flux (Figure 5 and Figure S4, Supporting Information);[28] the estimated PROS generated by **2** are $6.3 \pm 0.1\%$, $7 \pm 0.1\%$, and $13.5 \pm 1\%$ when physiabsorbed on EPG, C_8SH SAM, and $C_{16}SH$ SAM, respectively. As observed for other C*c*O mimics and porphyrin complexes,[26,38–40] **1** and **2** also show the same general trend of

increasing PROS generation with a decrease in the rate of electron transfer from the electrode. However, complex **3** shows the opposite trend, where on EPG the amount of PROS produced is $25 \pm 2\%$, i.e., only 75% of the O_2 was fully reduced by a $4e^-/4H^+$ process to give H_2O (Figure 5). In fact, this agrees well with the observed finding of $n = 3.4$ ($n = 3.5$ theoretically if 25% PROS is produced), that obtained from the $K-L$ analyses (vide supra). On C_8SH modified Au electrode, the magnitude of PROS is $10 \pm 1\%$ which further decreased to $4 \pm 1\%$ on further slowing down the electron transfer by employing a $C_{16}SH$ SAM modified surface (Figure 5, and Figure S5, Supporting Information). The diminished amount of $2e^-/2H^+$ reduction product (i.e., H_2O_2) with a decrease in ET rate is unprecedented for synthetic heme-Cu systems. To better understand this, SERRS-RDE experiments under steady state conditions have been performed for these catalysts.

SERRS-RDE data, collected on C_8SH SAM modified Ag disks, of the iron only catalyst **1** during steady state O_2 reduction, i.e., catalytic turnover (the electrode is held at -0.5 V vs Ag/AgCl) (Figure 6A, blue) shows the presence of four species in the high frequency region. The major species has ν_4 and ν_2 at 1362 and 1556 cm^{-1}, respectively, corresponding to HS Fe^{III} species (Figure 6D, red). There are two additional minor components having the ν_4 and ν_2 bands at 1350 and 1545 cm^{-1} (Figure 6D, green) and at 1375 and 1572 cm^{-1} (Figure 6D, black), respectively. The first minor species correspond to a HS Fe^{II} species and the other may correspond to a Fe^{IV}=O species as observed for other Fe–porphyrin complexes.[37,42,54] Note that a very weak Fe^{III} LS component in the ν_2 band could also be noticed at 1565 cm^{-1}. Under similar steady state turnover, the FeCu catalyst **2** also gives rise to a mixture of species as observed in this high frequency region (Figure 6B). Lorentzian fits of the ν_4 and ν_2 bands show the presence of three components (Figure 6E). The major species is a LS Fe^{III} complex with ν_4 and ν_2 bands at 1366 and 1567 cm^{-1}.[55,56] The other components correspond to a HS Fe^{II} species having ν_4 and ν_2 bands at 1349 and 1542 cm^{-1}, respectively, and a HS Fe^{III} species (very low population in steady state) with the ν_4 and ν_2 bands at 1359 and 1555 cm^{-1}, respectively (Figure 6E). SERRS-RDE data for **3** during steady state O_2 reduction shows the presence of LS Fe^{III}, LS Fe^{II}, and HS Fe^{II} species (Figure 6C, blue). The major component is the LS Fe^{III} species with the ν_4 and ν_2 bands at 1368 and 1569 cm^{-1} (Figure 6E). Fits to the ν_4 and ν_2 region clearly show the presence of bands at 1345 and 1544 cm^{-1} corresponding to a HS Fe^{II} species, whereas the bands at 1357 and 1559 cm^{-1} correspond to a LS Fe^{II} species (Figure 6E).[42] Note that a larger intensity of the LS Fe^{II} species is observed relative to the HS component that can be due to the higher resonance enhancement and/or a greater population, the latter being more likely.

SERRS-RDE data for complex **2** in the low frequency region shows the formation of an iron-peroxo intermediate (either bridged or terminal), which gives rise to an O–O stretching vibration (ν_{O-O}) at 819 cm^{-1} in $^{16}O_2$, shifting to 759 cm^{-1} in $^{18}O_2$ (Figure 7A). Unlike for simple Fe-porphyrin systems, a Fe^{IV}=O vibration was not observed. High-valent Fe^{IV}=O systems produced during O_2 reduction have been shown to be able to oxidize $K_4[Fe^{II}(CN)_6]$ present in solution and the $[Fe^{III}(CN)_6]^{-3}$ produced can be detected in the Pt ring in a RRDE setup as for Fe-porphyrin complexes.[52] Here, for **2**, the lack of significant current at the Pt ring (held at a negative potential where $[Fe^{III}(CN)_6]^{-3}$ can be reduced to $[Fe^{II}(CN)_6]^{-4}$) suggests that no Fe^{IV}=O is accumulated during O_2 reduction consistent with the lack of

Raman signal (Figure S6A, Supporting Information). When the SERRS-RDE experiment is performed in air saturated pD 7 buffer, the O–O peak appears at 819 cm^{-1} as observed in case of air saturated pH 7 buffer, which further suggests that the Fe-peroxo species formed, is a species with a peroxo bridge (i.e., Fe–O$_2^{2-}$–Cu), and not an iron hydroperoxide (Fe^{III}– OOH) complex (Figure S7, Supporting Information). Unfortunately, the low frequency region of the spectrum does not reveal corresponding Fe–O/Cu–O vibrations for the bridged-peroxo complex **2** (Figure S8A, Supporting Information).[57] However, the ν_{O-O} absolute value and its observed 60 cm^{-1} $^{16/18}$O shift (vide supra) are consistent with the O–O bond stretching frequency of Feperoxo species, excluding the possible formation of any high-valent Fe^{IV}=O species where a 25–30 cm^{-1} downshift is generally observed on ^{18}O substitution (Fe^{IV}=O is also excluded based on the ferrocyanide experiment discussed above).[58]

For complex **3** with imidazole "base", a prominent peak at 847 cm^{-1} appears, under steady state conditions in an air saturated pH 7 buffer, in the SERRS-RDE data which is shown to shift to 786 cm^{-1} (61 cm^{-1} $^{16/18}$O$_2$ downshift) in ^{18}O$_2$ (Figure 7B). Note that the magnitudes of the $^{16/18}$O isotope shifts (>60 cm^{-1}) for both the complexes are larger than the calculated values for the harmonic O–O diatomic oscillators which is likely due to the mixing or mode-coupling of the fundamental O–O stretching mode with porphyrin vibrations. A weak $^{16/18}$O$_2$ sensitive ν_{Fe-O} band could be identified for complex **3** at 545 cm^{-1}, which shifts to 524 cm^{-1} (21 cm^{-1} downshift) upon ^{18}O-substitution (Figure S8B, Supporting Information). Although another weak signal at 532 cm^{-1} is observed for the same complex **3** in ^{16}O$_2$, the shift in ^{18}O$_2$ is not detectable. Here too, no high-valent Fe^{IV}=O intermediates could be detected when carrying out the same K$_4$[Fe^{II}(CN)$_6$] assay (Figure S6B, Supporting Information). This relatively high energy of ν_{O-O} in complex **3** compared to complex **2** is likely due to the formation of an *end-on* (*μ*-1,2) bridged peroxo complex. This is because of the presence of a stronger *σ*-donor imidazole ligand in complex **3** which facilitates the formation of an *end-on* bridging peroxo moiety and not a *side-on* coordination, resulting in lower ν_{O-O} stretching vibrations, as also known from previous studies on similar C*c*O model complexes in organic media.[32,59,60]

DISCUSSION

A combination of electrochemical and spectroscopic techniques has been used to investigate the oxygen reactivity of C*c*O model complexes (i.e., a heme-Cu system with and without imidazole) physiabsorbed on electrode surfaces under physiological conditions. The parent heme-Cu ^{6}L-FeCu complex (**2**) selectively reduces O$_2$ by a 4e$^-$/4H$^+$ process under fast ET conditions (only 6% PROS) with a high overall k_{cat} for the ORR (4.49 × 10^6 M^{-1} s^{-1}), that being 1 order of magnitude higher than any other synthetic heme-Cu system.[6,28] The SERRS-RDE data obtained on this complex under steady state conditions reveal the presence of HS Fe^{II}, HS Fe^{III} and LS Fe^{III} species. The fact that the Fe^{II} center is in its HS state in the reduced complex **2** and was established to be in its LS Fe^{II} state in previously reported synthetic mimics of CcO likely explains the faster ORR kinetics observed in the former relative to the latter.[49] The additional vibration observed at 819 cm^{-1} which shifts to 759 cm^{-1} in ^{18}O$_2$ but does not shift on deuteration indicates that (a) a bridging peroxide is

involved in the mechanism and (b) the O–O bond cleavage of this peroxy species is likely to be a slow step in the mass transfer limited region (vide infra).[61] By contrast, the imidazole bound analogue of the parent heme-Cu [6]L-FeCu complex, [6]L-Fe(Im)Cu (imidazole bound trans to the bridging hydroxo ligand in the resting oxidized state), produces significant amounts of PROS (25%) during O_2 reduction on an EPG electrode. SERRS-RDE data on this complex shows the presence of a $^{16/18}O$ sensitive O–O vibration at 847 cm^{-1} (786 cm^{-1}) and Fe–O vibration at 545 cm^{-1} (524 cm^{-1}). Thus, a bridging peroxide ligand is an intermediate in the O_2 reduction cycle even with an imidazole axial ligand and the heterolytic O–O bond cleavage is a slow step as well. Note that the presence of *end-on* peroxide species has been demonstrated in X-ray structures of C*c*O[20,21,62] and their involvement in O_2 reduction has been proposed for "mixed valence" C*c*O (i.e., where just the FeCu active site is reduced).[13]

In the SERRS-RDE experiments, species for which the rate of formation is faster than its rate of decay will accumulate and can be detected. Analyses of marker bands indicate the accumulation of Fe[II] HS, Fe[II] LS and Fe[III] LS in the case of Fe–Cu complexes. SERRS-RDE is performed at a potential where the catalytic current is mass transfer limited, i.e., no change in the catalytic current occurs with an increase in the driving force and the current only depends on the supply of species from the aqueous phase. This implies that no species whose decay involves an electron transfer can be rate determining and accumulate during steady state at these potentials. This automatically excludes the possibility that an electron transfer step is the rate-determining step. The two components of the reaction (reduction of O_2 to H_2O) that diffuse from bulk solution to electrode surface are oxygen and protons. Consistently, it is observed that Fe[II] species (both HS and LS), which decay by binding oxygen (derived from bulk solvent), accumulate in the SERRS-RDE data. This is because of the formation of Fe[II] (**a**, Schemes 1 and 2) through reduction of Fe[III] (via ET from electrode) is faster at these potentials than O_2 binding. While O_2 binding in the distal pocket (i.e., containing the Cu) will lead to O–O cleavage and subsequent O_2 reduction, O_2 binding to the proximal site, replacing the axial water ligand, will likely result in the production of PROS (**c**, Scheme 1). Similarly, we believe the Fe[III] LS species observed is a bridging peroxide (**b**, Scheme 1 and c, Scheme 2) (the metal ligand region in the SERRS-RDE spectra also reflects the same) because its decay involves proton (from bulk) with subsequent O–O bond cleavage leading to the formation of high-valent compound I (**d**, Schemes 1 and 2). However, compound I cannot be isolated as an intermediate during steady state, perhaps because of the immediate reduction of this high valent species by electron transfer from the electrode which is held at −0.5 V vs Ag/AgCl during SERRS-RDE experiments i.e. its decay is faster than its formation precluding its accumulation during steady state. Thus, the data indicate that both O_2 binding and heterolytic cleavage of O–O bond are slow. However, from the greater intensity LS Fe[III] component in the ν_4 and ν_2 region relative Fe[II] component, we propose that decay of the bridging peroxide species via protonation is slower than decay of Fe[II] resulting from O_2 binding.

The relative values of the $\nu_{O–O}$ suggest that the peroxo intermediate formed under steady state conditions in the [6]L-FeCu complex has a *side-on* coordination, whereas the one formed in the [6]L-Fe(Im)Cu analogue is bound in an *end-on* geometry. These assignments are in

good agreement with the previously reported homogeneous data where similar shifts are observed upon switching a *side-on* to *end-on* intermediate.[31,32,59] Considering the fact that the peroxo adduct of the [6]L-FeCu complex is 6C LS (based on the ν_4 and ν_2 values), the binding motif of the bridging *side-on* peroxo to the Fe and Cu centers is likely $\mu–\eta^1:\eta^2$ (η^2 at Cu and η^1 at Fe; **b**, Scheme 1) in an aqueous environment and not $\mu–\eta^2:\eta^1$ as observed in organic solvents.[31,32,59] The $\nu_{O–O}$ observed in the SERRS-RDE data, here, in an aqueous environment, is ~30 cm^{-1} higher than the values observed in structurally characterized high-spin Fe– ($\mu–\eta^2:\eta^1$-peroxo)–Cu model compounds in organic solution.[31,33] These differences may arise from differences in polarity of the medium or hydrogen bonding from water, or due to the change from high-spin to low-spin, or of course due to proposed change to being *side-on* to Cu (Scheme 1).

Complex **3** shows selective 4e$^-$/4H$^+$ O$_2$ reduction under slow ET flux (<4% PROS when physiabsorbed on C$_{16}$SH modified SAM on Au) whereas under fast ET, where complex **2** and all known heme-Cu complexes show 4e$^-$/4H$^+$ O$_2$ reduction, this complex with an axial imidazole ligand shows significant 2e$^-$/2H$^+$ reduction of O$_2$. SERRS-RDE data on this complex reveals accumulation of LS Fe^{II} species; presumably with a water molecule as the sixth axial ligand (**a**, Scheme 2). Ferrous porphyrins in the LS ground state are known to have sluggish rates of O$_2$ binding.[40,47] It is likely that under fast ET on EPG (i.e., when k_{ET} > k_{O2} for the LS Fe^{II} center), the distal Cu reduces O$_2$ to produce PROS (**b**, Scheme 2). As the ET rate is slowed and becomes comparable to or even slower than the O$_2$ binding rate to LS Fe^{II} (i.e., $k_{ET} \approx k_{O2}$ or $k_{ET} < k_{O2}$), the O$_2$ (slowly) binds to iron and the 4e$^-$/4H$^+$ ORR proceeds via a bridging peroxo intermediate (**c**, Scheme 2). The ferrous center in its LS state may also reduce O$_2$ via outer sphere O$_2$ reduction by 1e$^-$ when the ET rate is fast.[51,63,64] Thus, the product, i.e., water, can bind the heme iron in its reduced state and act as a competitive inhibitor of the substrate, O$_2$.[47,65,66] For facile O$_2$ reduction, it is important that the water formed is released from the active site; this effect may also be operative in the native CcO enzyme active site through proper water channelling.[3,65]

CONCLUSION

In summary, bridging peroxo intermediates are shown to be involved during electrocatalytic O$_2$-reduction in aqueous media by heme-Cu complexes which are otherwise known to form such Fe–O$_2{}^{2-}$–Cu species in organic solvents. The kinetics of O$_2$-reduction compare fairly well with those of the heme–Cu complexes that are proposed not to involve a bridging peroxide type intermediates. Thus, pathways involving bridging peroxide intermediates can lead to facile and selective 4e$^-$/4H$^+$ O$_2$-reduction.

EXPERIMENTAL DETAILS

Materials

All reagents were of the highest grade commercially available and were used without further purification. Octanethiol (C$_8$SH), hexadecanethiol (C$_{16}$SH), potassium hexafluorophosphate (KPF$_6$), chloroform (CHCl$_3$) and all buffers were purchased from Sigma-Aldrich. Disodium hydrogen phosphate dihydrate (Na$_2$HPO$_4 \cdot$ 2H$_2$O), potassium chloride (KCl), imidazole (Im), conc. sulfuric acid (H$_2$SO$_4$), and deuterium oxide (D$_2$O) were purchased from Merck.

Au wafers were obtained from Platypus Technologies (1000 Å of Au on 50 Å of Ti adhesion layer on top of a Si(III) surface). Edge Plane Graphite (EPG), Au disks for the RRDE experiments and Ag disks for SERRS experiments were purchased from Pine Instruments.

Instrumentation

UV–vis absorption data were taken in an Agilent technologies spectrophotometer model 8453 fitted with a diode-array detector. All electrochemical experiments were performed using a CH Instruments (model CHI710D Electrochemical Analyzer). A Biopotentiostat, reference electrodes and a Teflon plate material evaluating cell (ALS Japan) were purchased from CH Instruments. The rotating ring disk electrochemical (RRDE) setup from Pine Research Instrumentation (E6 series ChangeDisk tips with AFE6M rotor) was used to obtain the RRDE data. Surface Enhanced Resonance Raman data were collected with a Trivista 555 spectrograph (Princeton Instruments) using 413.1 nm excitation from a Kr^+ laser (Coherent, Sabre Innova SBRC-DBW-K). Mass spectra were recorded by a QTOF Micro YA263 instrument.

Synthesis

The heme-(μ-hydroxo)-copper complex [6]L-FeCu (**2**) and its copper free heme analogue [6]L-Fe (**1**) were synthesized as reported in the literature.[67,68] The imidazole adduct of [6]L-FeCu, [6]L-Fe(Im)Cu (**3**), was prepared by adding imidazole dissolved in $CHCl_3$ to a 1 mM solution of **2** in $CHCl_3$. The formation of the complex was monitored by UV–vis (Figure S1B, Supporting Information) and TOF MS ES+ (Figure S1C) and was also confirmed by rR spectroscopy (Figure S1A). Note that since imidazole has been added to the complex **2** (as synthesized) in a noncoordinating organic medium, it binds to the open face of the heme as a sixth ligand (i.e., trans to the bridging hydroxo moiety, see Figure 2).

Construction of Electrodes

Formation of Self-Assembled Monolayer (SAM)—Au wafers and disks were cleaned electrochemically by sweeping several times between 1.5 V to −0.3 V (vs. Ag/AgCl) in 0.5 M H_2SO_4. Ag disks were cleaned in alumina (size: 1, 0.3 and 0.05 μm) and then roughened in 0.1 M KCl solution as described in literature. SAM solutions were prepared in ethanol using 0.4 mM concentration of the corresponding alkanethiols. Freshly cleaned Au wafers, disks and freshly roughened Ag disks were initially rinsed with tripled distilled water, ethanol, purged with N_2 gas and then immersed in the depositing solution of C_8SH or $C_{16}SH$ in ethanol for 4 and 20 h, respectively.

Physiabsorption of Catalysts on to EPG and SAM—EPG disks were cleaned on silicon carbide (SiC) grit paper followed by sonication in ethanol and dried under N_2 gas. The disks were then mounted on a platinum ring disk assembly (Pine Instruments). The solutions of the catalysts were prepared in chloroform followed by drop-casting on the EPG electrode for 30 min for complete loading. The surfaces were then thoroughly rinsed with chloroform followed by ethanol and triply distilled deionized water and dried before CV, RDE and RRDE experiments. In case of modified Au and roughened Ag disks, the disks were taken out of the depositing solutions, rinsed with ethanol and chloroform and then mounted on the RRDE setup. The catalysts were loaded as described for EPG. After each

respective loading, the surfaces were thoroughly rinsed with chloroform, ethanol and triply distilled water before carrying out electrochemical or SERRS/SERRS-RDE experiments.

Electrochemical Experiments

All electrochemical experiments were carried out in pH 7 buffer (unless otherwise mentioned) containing 100 mM $Na_2HPO_4.2H_2O$ and 100 mM KPF_6 (supporting electrolyte) using Pt wire as the counter electrode and Ag/AgCl as the reference electrode.

Cyclic Voltammetry

The CVs of the catalysts were obtained by physiabsorbing the complexes on EPG electrodes under anaerobic conditions in deoxygenated buffer at a scan rate of 50 mV/s.

Coverage Calculation

The coverage for a particular redox couple is estimated by taking the average of the integrated area under the corresponding oxidation and reduction currents of the respective species obtained from their reversible voltammogram. The experiments were repeated three times and an average value with standard deviation has been presented.

Ring Disk Electrochemistry (RDE)

The RDE measurements were performed on a CHI 700D bipotentiostat with a Pine Instruments Modulated speed rotor fitted with an E6 series Changedisk tip. The complexes were physiabsorbed on the disks as described earlier. The Koutecky–Levich (*K–L*) experiments were performed for all the complexes at the following rotations: 100, 200, 300, 400, 500, and 600 rpm. The second order rate of catalysis (k_{cat}) can be evaluated from the intercept of the *K–L* plot (see Figure 4) using the equation $i_K = nFA[O_2]k_{cat}\Gamma_{catalyst}$ where i_K is expressed as the inverse of the intercept obtained upon plotting I^{-1} at different rotation rates with respect to $\omega^{-1/2}$ and $\Gamma_{catalyst}$ is the surface coverage of the catalyst obtained from the integrated current of the CV taken under anaerobic conditions.

Rotating Ring Disk Electrochemistry (RRDE): Partially Reduced Oxygen Species (PROS) Detection and Calculation

The platinum ring and the Au disk were both polished using alumina powder (grit sizes: 1, 0.5, and 0.03 μm) and electrochemically cleaned and inserted into the RRDE tip which was then mounted on the rotor and immersed into a cylindrical glass cell equipped with Ag/AgCl reference and Pt counter electrodes (Figure 8A). In this technique, the potential of the disk is swept from positive to negative and when O_2 is reduced, any H_2O_2, i.e., a 2e⁻ reduction product of O_2, produced in the working disk electrode is radially diffused to the encircling Pt ring, which is held at a constant potential and oxidizes the H_2O_2 back to O_2 (Figure 8B). The ratio of the 2e⁻/2H⁺ current (corrected for collection efficiency) at the ring and the catalytic current at the disk is expressed as PROS and it provides an *in situ* measure of the 2e⁻/2H⁺ reduction side reaction. The collection efficiency (CE) of the RRDE setup was measured in a 2 mM $K_3[Fe^{III}(CN)_6]$ and 0.1 M KNO_3 solution at a 10 mV/s scan rate and 300 rpm rotation speed. A 20 ± 2% CE was generally recorded during these experiments.

The potential at which the ring was held during the collection efficiency experiments at pH 7 for detecting H_2O_2 was obtained from literature.[69]

Surface Enhanced Resonance Raman Spectroscopy Coupled with RDE (SERRS-RDE)

Ag disks were cleaned using Alumina powder (grit sizes 1, 0.3, and 0.05 μm) and then roughened in a 0.1 M KCl solution using reported procedures and then immersed in SAM solutions. The catalysts were loaded as mentioned earlier. The roughened modified Ag disks were then inserted into the RRDE setup for the collection of SERRS-RDE data. The detailed SERRS-RDE set up along with the technique has been recently published.[37] The disks were held at 0 V vs Ag/AgCl to obtain the oxidized spectra and at −0.5 V vs Ag/AgCl to obtain the reduced spectra and the spectra under steady state conditions under anaerobic and aerobic conditions, respectively. Experiments were done using an excitation wavelength 413.1 nm and the power used at the electrode surface was 8–10 mW. All the SERRS spectra have been normalized using the characteristic buffer peaks which appear at 742 cm^{-1} (coming from electrolyte KPF_6) and 951 cm^{-1} (symmetric ν_{P-O}), respectively.

Supplementary Material

Refer to Web version on PubMed Central for supplementary material.

Acknowledgments

References

1. Yoshikawa S, Shimada A. Chem Rev. 2015; 115:1936. [PubMed: 25603498]

2. Kim E, Chufán EE, Kamaraj K, Karlin KD. Chem Rev. 2004; 104:1077. [PubMed: 14871150]

3. Ferguson-Miller S, Babcock GT. Chem Rev. 1996; 96:2889. [PubMed: 11848844]

4. Babcock GT, Wikstrom M. Nature. 1992; 356:301. [PubMed: 1312679]

5. Collman JP, Ghosh S, Dey A, Decreau RA, Yang Y. J Am Chem Soc. 2009; 131:5034. [PubMed: 19317484]

6. Collman JP, Decreau RA. Chem Commun. 2008:5065.

7. Chufan EE, Puiu SC, Karlin KD. Acc Chem Res. 2007; 40:563. [PubMed: 17550225]

8. Rousseau DL. Nature. 1999; 400:412. [PubMed: 10440367]

9. Anson FC, Shi C, Steiger B. Acc Chem Res. 1997; 30:437.

10. Blomberg MRA, Siegbahn PEM. Biochim Biophys Acta, Bioenerg. 2014; 1837:1165.

11. Svensson-Ek M, Abramson J, Larsson G, Tõrnroth S, Brzezinski P, Iwata S. J Mol Biol. 2002; 321:329. [PubMed: 12144789]

12. Tsukihara T, Aoyama H, Yamashita E, Tomizaki T, Yamaguchi H, Shinzawa-Itoh K, Nakashima R, Yaono R, Yoshikawa S. Science. 1996; 272:1136. [PubMed: 8638158]

13. Proshlyakov DA, Pressler MA, Babcock GT. Proc Natl Acad Sci U S A. 1998; 95:8020. [PubMed: 9653133]

14. Kaila VRI, Verkhovsky MI, Wikström Mr. Chem Rev. 2010; 110:7062. [PubMed: 21053971]

15. Proshlyakov DA, Pressler MA, DeMaso C, Leykam JF, DeWitt DL, Babcock GT. Science. 2000; 290:1588. [PubMed: 11090359]

16. Karlin KD, Kim E. Chem Lett. 2004; 33:1226.

17. Han S, Takahashi S, Rousseau DL. J Biol Chem. 2000; 275:1910. [PubMed: 10636892]

18. Liu JG, Naruta Y, Tani F. Chem Eur J. 2007; 13:6365. [PubMed: 17503416]

19. Halime Z, Kotani H, Li Y, Fukuzumi S, Karlin KD. Proc Natl Acad Sci U S A. 2011; 108:13990. [PubMed: 21808032]

20. Aoyama H, Muramoto K, Shinzawa-Itoh K, Hirata K, Yamashita E, Tsukihara T, Ogura T, Yoshikawa S. Proc Natl Acad Sci U S A. 2009; 106:2165. [PubMed: 19164527]

21. Tiefenbrunn T, Liu W, Chen Y, Katritch V, Stout CD, Fee JA, Cherezov V. PLoS One. 2011; 6:e22348. [PubMed: 21814577]

22. Koepke J, Olkhova E, Angerer H, Mäller H, Peng G, Michel H. Biochim Biophys Acta, Bioenerg. 2009; 1787:635.

23. Kaila VRI, Oksanen E, Goldman A, Bloch DA, Verkhovsky MI, Sundholm D, Wikstrom M. Biochim Biophys Acta, Bioenerg. 2011; 1807:769.

24. Sakaguchi M, Shinzawa-Itoh K, Yoshikawa S, Ogura T. J Bioenerg Biomembr. 2010; 42:241. [PubMed: 20354773]

25. Although the PDB ID: 3ABM does not report the *side-on* configuration, upon analyzing the crystal structure, the Cu–O distances between the Cu and both oxygen atoms of the bridging peroxides are found to be below 2.6 Å (2.51 and 2.59 Å, respectively). This is why we show Figure 1A depicted with a *side-on* geometry.

26. Collman JP, Devaraj NK, Decréau RA, Yang Y, Yan YL, Ebina W, Eberspacher TA, Chidsey CED. Science. 2007; 315:1565. [PubMed: 17363671]

27. Collman JP, Boulatov R, Sunderland CJ, Fu L. Chem Rev. 2004; 104:561. [PubMed: 14871135]

28. Boulatov R, Collman JP, Shiryaeva IM, Sunderland CJ. J Am Chem Soc. 2002; 124:11923. [PubMed: 12358536]

29. Ricard D, Andrioletti B, Boitrel B, L'Her M. Chem Commun. 1999; 1523

30. Collman JP, Fu L, Herrmann PC, Zhang X. Science. 1997; 275:949. [PubMed: 9020071]

31. Garcia-Bosch I, Adam SM, Schaefer AW, Sharma SK, Peterson RL, Solomon EI, Karlin KD. J Am Chem Soc. 2015; 137:1032. [PubMed: 25594533]

32. Kieber-Emmons MT, Qayyum MF, Li Y, Halime Z, Hodgson KO, Hedman B, Karlin KD, Solomon EI. Angew Chem, Int Ed. 2012; 51:168.

33. Ghiladi RA, Huang H-w, Moenne-Loccoz P, Stasser J, Blackburn NJ, Woods AS, Cotter RJ, Incarvito CD, Rheingold AL, Karlin KD. J Biol Inorg Chem. 2005; 10:63. [PubMed: 15583964]

34. Liu J-G, Ohta T, Yamaguchi S, Ogura T, Sakamoto S, Maeda Y, Naruta Y. Angew Chem, Int Ed. 2009; 48:9262.

35. Ohta T, Liu J-G, Naruta Y. Coord Chem Rev. 2013; 257:407.

36. Collman JP, Rapta M, Bröring M, Raptova L, Schwenninger R, Boitrel B, Fu L, L'Her M. J Am Chem Soc. 1999; 121:1387.

37. Sengupta K, Chatterjee S, Samanta S, Dey A. Proc Natl Acad Sci U S A. 2013; 110:8431. [PubMed: 23650367]

38. Chatterjee S, Sengupta K, Samanta S, Das PK, Dey A. Inorg Chem. 2015; 54:2383. [PubMed: 25695312]

39. Samanta S, Sengupta K, Mittra K, Bandyopadhyay S, Dey A. Chem Commun. 2012; 48:7631.

40. Chatterjee S, Sengupta K, Samanta S, Das PK, Dey A. Inorg Chem. 2013; 52:9897. [PubMed: 23961832]

41. The cyclic voltammograms for complexes investigated are broad which may reflect heterogeneous constructs suggesting the presence of multiple species on the electrode as observed from the mixture of marker bands for the adsorbed species in the oxidized and reduced SERRS spectra.

42. Burke JM, Kincaid JR, Peters S, Gagne RR, Collman JP, Spiro TG. J Am Chem Soc. 1978; 100:6083.

43. Abe M, Kitagawa T, Kyogoku Y. Chem Lett. 1976; 5:249.

44. Weidinger IM. Biochim Biophys Acta, Bioenerg. 2015; 1847:119.

45. Upon reduction, new peak in the ν_3 region for complex 1 was not observed.

46. A Lorentzian fit of the spectrum for reduced complex 2 shows the presence of minor LS Fe^{II} component as well having ν_4, ν_3, and ν_2 bands at 1359, 1444, 1561 cm^{-1}, respectively, which is likely due to the formation of a bis-aqua complex (Figure 3E).

47. Collman JP, Decreau RA, Dey A, Yang Y. Proc Natl Acad Sci U S A. 2009; 106:4101. [PubMed: 19246375]

48. Maillard P, Schaeffer C, Tetreau C, Lavalette D, Lhoste JM, Momenteau M. J Chem Soc, Perkin Trans 2. 1989; 1437

49. Saveant, J-M. Elements of Molecular and Biomolecular Electrochemistry. Wiley-Interscience; Hoboken, NJ: 2006.

50. Bard, AJ.; Faulkner, LR. Electrochemical Methods. J. Wiley; New York: 1980.

51. Momenteau M, Reed CA. Chem Rev. 1994; 94:659.

52. Sengupta K, Chatterjee S, Samanta S, Bandyopadhyay S, Dey A. Inorg Chem. 2013; 52:2000. [PubMed: 23356644]

53. Chidsey CED. Science. 1991; 251:919. [PubMed: 17847385]

54. Hashimoto S, Mizutani Y, Tatsuno Y, Kitagawa T. J Am Chem Soc. 1991; 113:6542.

55. Rousseau DL, Han S, Song S, Ching Y-C. J Raman Spectrosc. 1992; 23:551.

56. Das TK, Pecoraro C, Tomson FL, Gennis RB, Rousseau DL. Biochemistry. 1998; 37:14471. [PubMed: 9772174]

57. In the low frequency region, no distinct Fe–O/Cu–O vibrations could be observed, which is likely because of strong background from heme in this region.

58. However, the use of scrambled isotope would provide a definite assessment for the assignment of peroxo or ferryl complex.

59. Kieber-Emmons MT, Li Y, Halime Z, Karlin KD, Solomon EI. Inorg Chem. 2011; 50:11777. [PubMed: 22007669]

60. Halime Z, Kieber-Emmons MT, Qayyum MF, Mondal B, Gandhi T, Puiu SC, Chufan EE, Sarjeant AAN, Hodgson KO, Hedman B, Solomon EI, Karlin KD. Inorg Chem. 2010; 49:3629. [PubMed: 20380465]

61. Rate-determining step is defined as the step(s) having higher kinetic barriers than other steps involved in a particular catalytic cycle.

62. Du W-GH, Noodleman L. Inorg Chem. 2013; 52:14072. [PubMed: 24262070]

63. Wallace WJ, Houtchens RA, Maxwell JC, Caughey WS. J Biol Chem. 1982; 257:4966. [PubMed: 6279655]

64. Stanbury DM, Haas O, Taube H. Inorg Chem. 1980; 19:518.

65. Shimokata K, Katayama Y, Murayama H, Suematsu M, Tsukihara T, Muramoto K, Aoyama H, Yoshikawa S, Shimada H. Proc Natl Acad Sci U S A. 2007; 104:4200. [PubMed: 17360500]

66. Chang CJ, Chang MCY, Damrauer NH, Nocera DG. Biochim Biophys Acta, Bioenerg. 2004; 1655:13.

67. Ghiladi RA, Ju TD, Lee D-H, Mönne-Loccoz P, Kaderli S, Neuhold Y-M, Zuberbühler AD, Woods AS, Cotter RJ, Karlin KD. J Am Chem Soc. 1999; 121:9885.

68. Obias HV, van Strijdonck GPF, Lee D-H, Ralle M, Blackburn NJ, Karlin KD. J Am Chem Soc. 1998; 120:9696.

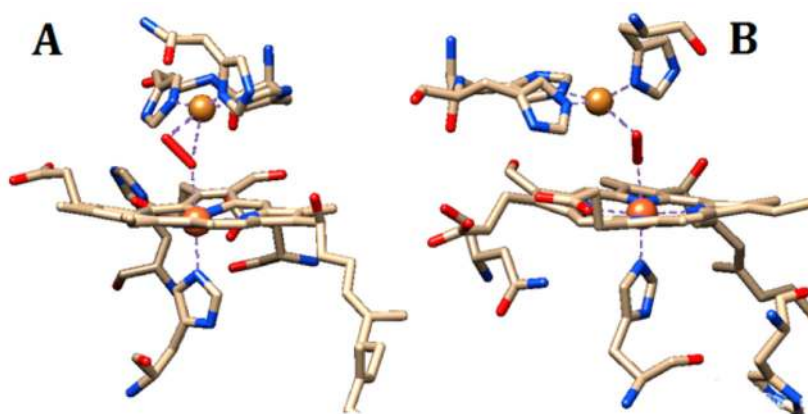69. Zhang Y, Wilson GS. J Electroanal Chem. 1993; 345:253.

Figure 1.
Binuclear active site structures of C*c*O showing (A) *side-on* ($\mu-\eta^1:\eta^2$) (η^1 at Fe center and η^2 at Cu center) (PDB ID: 3ABM)[25] and (B) *end-on* (μ-*1, 2*) (PDB ID: 3S8F) bridging peroxo complexes.
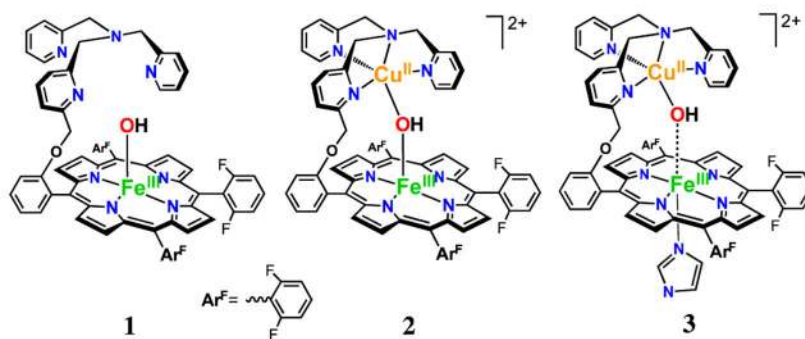
Figure 2.
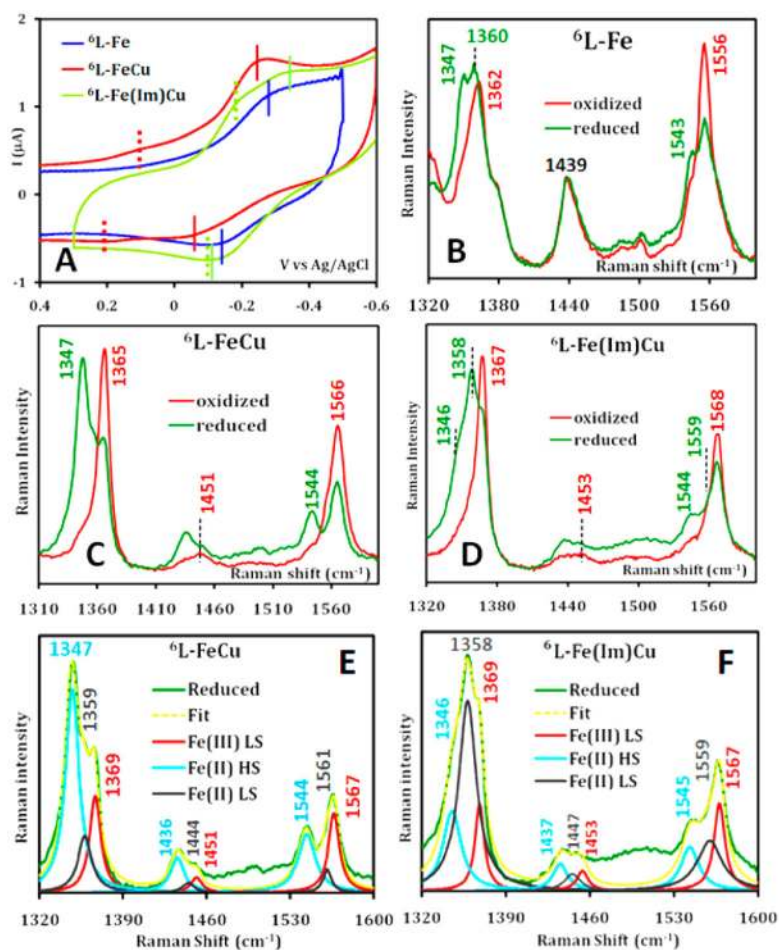6L-Fe (**1**), 6L-FeCu (**2**), and 6L-Fe(Im)Cu (**3**) are the synthetic model complexes used for this study.

Figure 3.
(A) CV data of complexes **1** (blue), **2** (red), and **3** (green) physiabsorbed on an EPG electrode in deoxygenated pH 7 buffer under an argon atmosphere at a scan rate of 50 mV/s using Ag/AgCl as reference and Pt wire as counter electrodes. SERRS data of **1** (B), **2** (C), and **3** (D), physiabsorbed on a C_8SH modified Ag disk, under oxidizing (red) and reducing (green) conditions in pH 7 buffer under anaerobic conditions at a constant rotation rate of 200 rpm. (E) and (F) are the ν_4, ν_3, and ν_2 bands of the spectra obtained at reducing conditions of complex **2** and **3**, respectively, along with their Lorentzian fits showing different components.
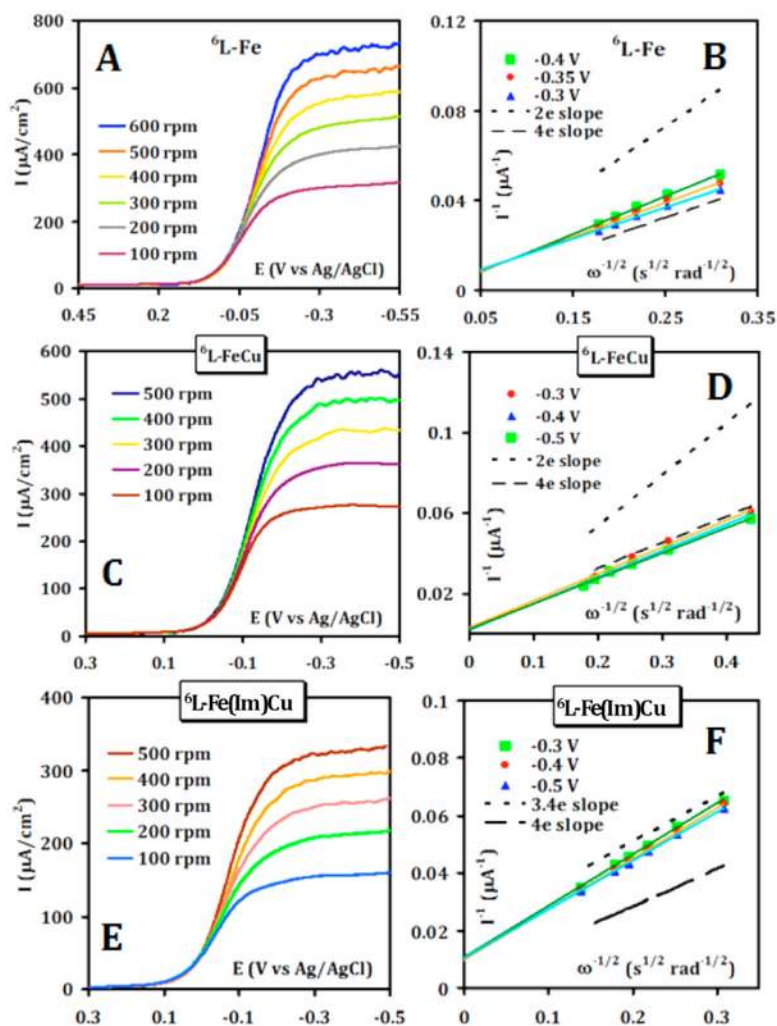
Figure 4.
LSV of **1** (A), **2** (C), and **3** (E) physiabsorbed on EPG in air saturated pH 7 buffer at a scan rate of 50 mV/s at multiple rotations using Ag/AgCl as reference and Pt wire as counter electrodes. The *K–L* plots of the respective catalysts at various potentials are given in (B), (D), and (F). The theoretical plots for 2e⁻, 3.4e⁻, and 4e⁻ processes are also indicated in the figures.
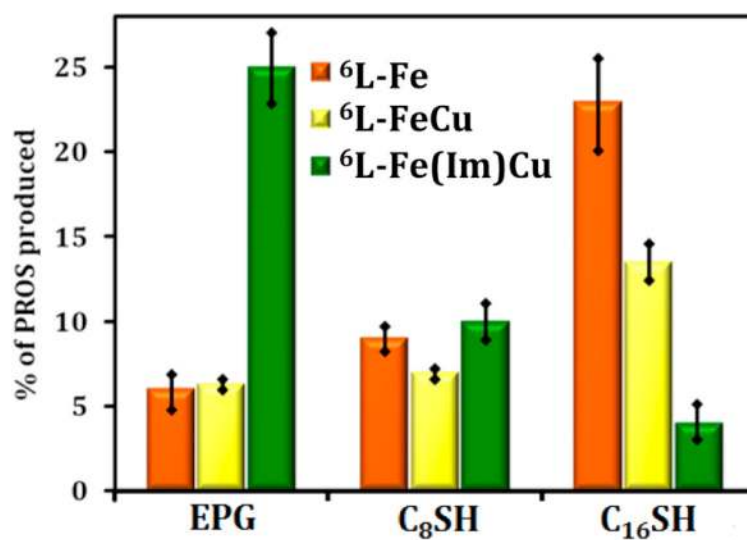
Figure 5.
Percentage of PROS formed by the catalysts **1** (red), **2** (yellow), and **3** (green) in air saturated pH 7 buffer under fast (EPG), slow (C_8SH SAM on Au), and very slow ($C_{16}SH$ SAM on Au) electron fluxes measured by a RRDE experiment using Ag/AgCl reference and Pt wire counter electrodes. Rotation speed = 300 rpm, scan rate = 10 mV/s.
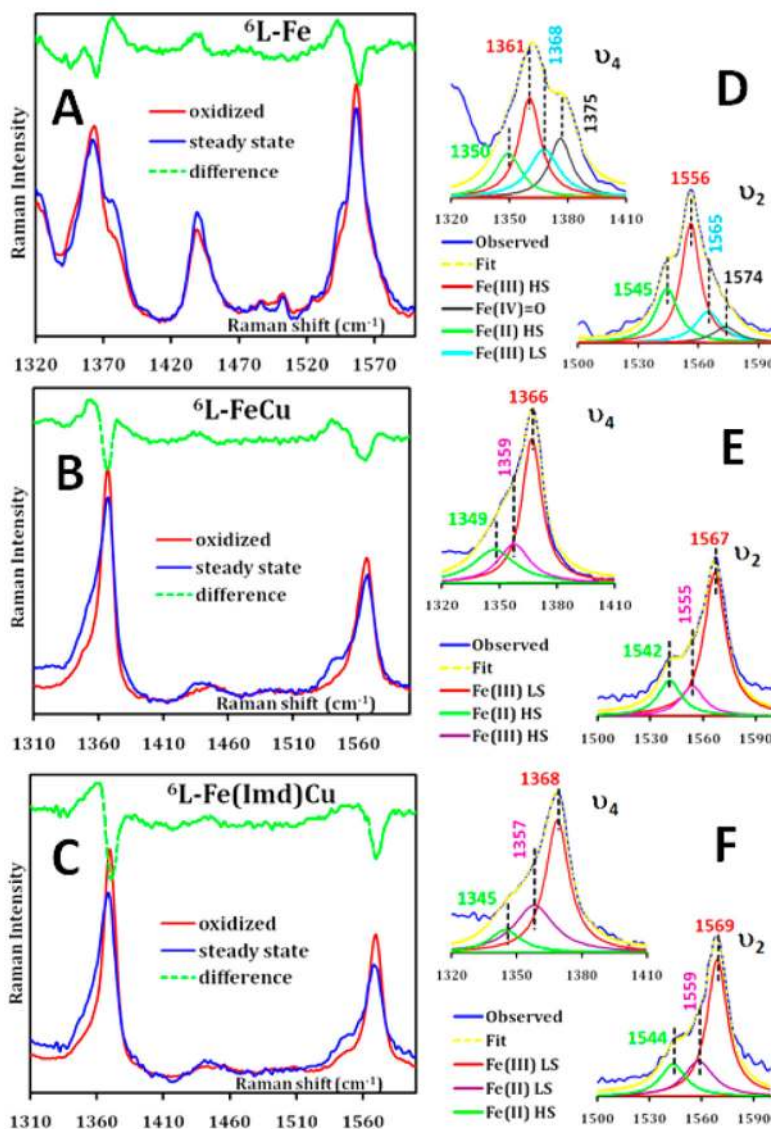
Figure 6.
SERRS-RDE data for complexes **1** (A), **2** (B) and **3** (C) in the high frequency region at oxidized (red) and steady state conditions (blue) in air saturated pH 7 buffer under aerobic conditions at a constant rotation rate of 200 rpm. The difference spectra are shown in green. The ν_4 and ν_2 bands of the spectra obtained during steady state O_2 reduction of complex **1**, **2**, and **3** along with their Lorentzian fits showing different components are given in (D), (E), and (F), respectively.
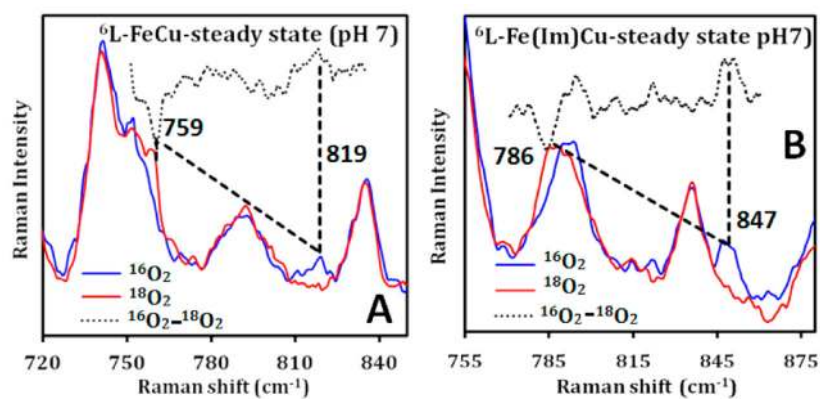
Figure 7.
SERRS-RDE data in the low frequency region under steady state conditions in the presence of air and $^{18}O_2$ saturated pH 7 buffer for complex **2** (A) and complex **3** (B) on C_8SH modified Ag surfaces. The difference spectra are shown in dotted line (black).
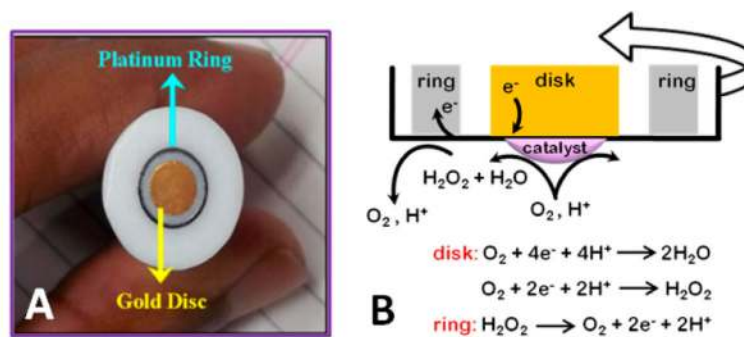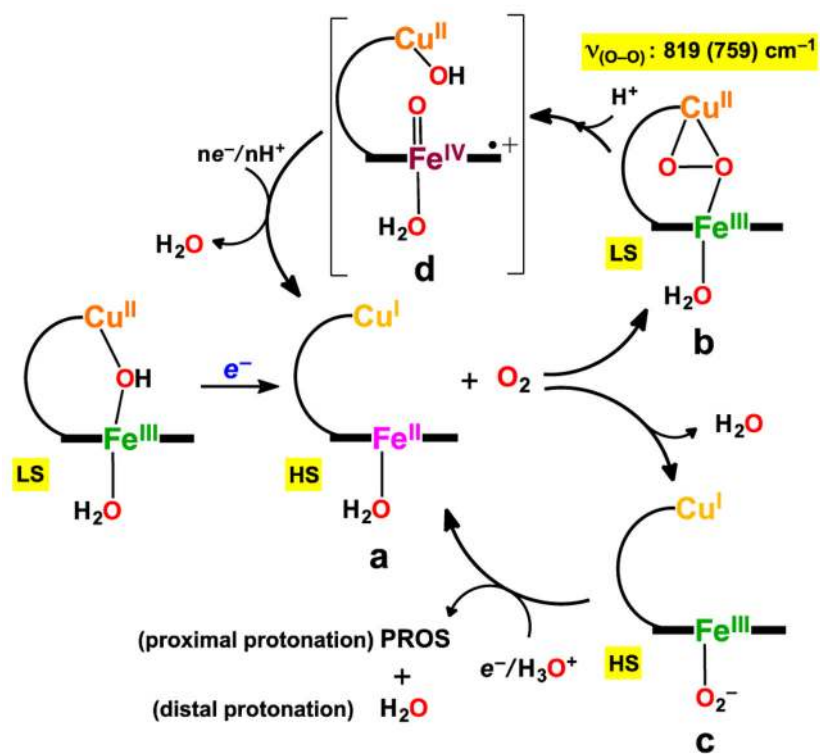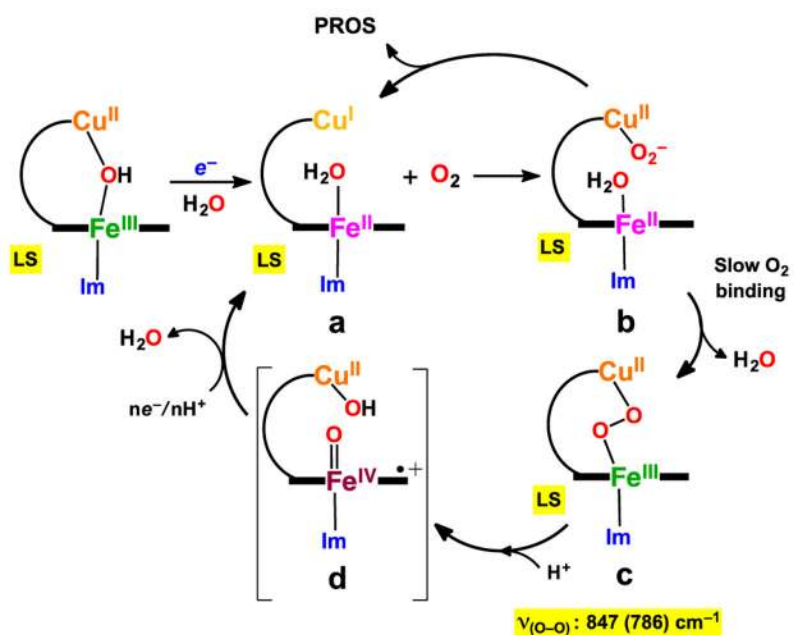
Figure 8.
(A) RRDE assembly showing the Au disk and Pt ring. (B) Schematic representation of PROS detection mechanism by a RRDE setup.

Scheme 1.
Plausible Mechanistic Pathways during Steady State O_2-Reduction by Complex 2

Scheme 2.
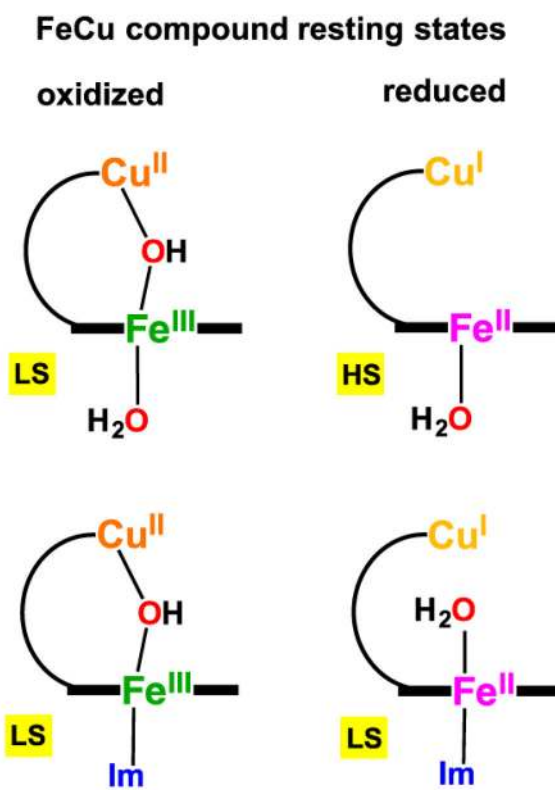Plausible Mechanistic Pathways during Steady State O_2-Reduction by Complex 3

Chart 1.